

31<sup>ST</sup> EUROPEAN ROTORCRAFT FORUM

Session B2-C2 / CFD Complete  
Paper 2

ACTUATOR DISC FOR HELICOPTER ROTORS  
IN THE UNSTRUCTURED FLOW SOLVER TAU

R. Schweikhard

F. Le Chuiton

DLR

Institute of Aerodynamics and Flow Technology  
Braunschweig – Germany

September 13-15th, 2005

Firenze

Italy

# ACTUATOR DISC FOR HELICOPTER ROTORS IN THE UNSTRUCTURED FLOW SOLVER TAU

Roland Schweikhard  
Frédéric Le Chuiton  
DLR – Institute of Aerodynamics and Flow Technology  
Braunschweig, Germany

## Abstract

Motivated by the demand for a fast flow simulation tool that takes the interaction between rotor and helicopter fuselage into account, an actuator disc boundary condition suited for helicopter rotors in forward flight has been implemented in the unstructured DLR TAU code. The time-averaged effect of the rotor, which accelerates the flow and adds energy to the fluid is imposed using source terms in the Navier-Stokes equations where the actuator disc is located in the grid. The transfer of this approach, previously implemented in the structured DLR FLOWer code, involved adapting the strategy to the unstructured framework. It is shown that propeller simulation results are in accordance to FLOWer results and simple 1D theory predictions. Moreover, rotor in forward flight cases prove the robustness of the implementation and resemble FLOWer results. Further development involved testing the implementation in parallel mode and a more sophisticated rotor force distribution is applied instead of a constant pressure jump. Finally, a comparison of the viscous flow field around the EC145 helicopter computed by TAU and FLOWer is performed. It shows that there is good agreement between the two codes in predicting the effect of the actuator disc on the fuselage pressure distribution.

$\vec{n}$	unit normal vector
$N_n$	number of neighbors
$p$	pressure
$\vec{Q}_\Omega$	source vector
$\vec{Q}_S$	surface source tensor
$R$	rotor radius, inner rotor radius $R_i$
$\vec{R}$	residual vector
$Re$	Reynolds number
$\vec{S}$	face vector with face area $S$
$T$	thrust
$t$	time
$\vec{U}$	vector of conservative variables
$\vec{V}$	velocity vector, components $(u, v, w)$

## Greek Symbols

$\alpha$	incidence angle
$\rho$	density
$\omega$	rotation frequency
$\Omega$	volume
$\psi$	azimuthal blade angle

## Subscripts

AD	actuator disc plane
eff	refers to the true disc area
tip	rotor blade tip
$\infty$	free-stream condition
0	stagnation condition

## Nomenclature

### Symbols

$A$	area
$c$	speed of sound
$c_p$	pressure coefficient
$C_l, C_d$	lift and drag coefficient
$C_T$	thrust coefficient
$d$	actuator disc diameter
$\vec{D}$	artificial dissipation operator
$E$	total specific energy
$\vec{f}$	force density vector
$\vec{F}$	force vector
$\vec{F}$	flux tensor
$m$	mass, face index
$M$	Mach number

## Introduction

Nowadays CFD is routinely used in industry as a design and analysis tool. The comparison of different designs enables the evaluation of a potential performance increase. Compared to wind-tunnel experiments CFD allows a much more detailed view of flow phenomena. It therefore also provides explanations for the potential performance increases. However, industry demands faster and more accurate analysis tools that enable quick turnaround times.

In the framework of helicopter design a major challenge is flow unsteadiness due to rotating blades. Although there exist some low-fidelity rotor modeling

tools such as blade element methods and panel methods, they are not suited for an accurate computation of the viscous interaction between rotor and fuselage. Such analysis demands high-fidelity methods, i.e. methods based on a solution of the Euler or Navier-Stokes equations, that compute both vortices and the pressure field accurately. In general, modeling helicopters including rotors is nowadays possible following two different approaches.

The first approach is to compute the unsteady flow field by taking into account each rotating blade. This is accomplished using the Chimera technique, with separate rotor blade grids moving over a fuselage background grid ([1],[2]). However, this approach is extremely time consuming and therefore not suited for everyday industrial applications.

Drastically reduced geometrical complexity, computational time and user input can be achieved with a second approach: modeling the flow field in a quasi-steady sense by employing an actuator disc. An actuator disc represents the area that the rotor blades sweep over during each revolution and is meant to impose the time-averaged effect of the rotor blades. An actuator disc, suited for rotor in forward flight cases, has been successfully implemented into the structured DLR FLOWer solver by Le Chuiton [3] and at ONERA by Bettshart [4].

While the FLOWer actuator disc produces high-quality flow solutions (see computation of EC145 [5]) a significant amount of work is involved to obtain these. The generation of structured grids around complex bodies such as a helicopter fuselage requires a lot of experience and time. Furthermore the Chimera technique is used to place main and tail rotor actuator discs into the fuselage grid. This requires special attention when actuator discs are close to the helicopter fuselage since grid holes need to be defined.

To reduce the complexity associated with structured grid generation it was decided to transfer the actuator disc implementation approach from FLOWer to the unstructured DLR TAU Solver. User input and the associated CAD work for the generation of an unstructured grid around a complex geometry is much lower. Furthermore, unstructured grids enhance the amount of geometrical complexity that can be modeled such as antennas, the rotor mast and so on.

## Numerics

### Conservation Laws and Source Terms

To understand the implementation concepts of the actuator disc boundary condition it is worthwhile taking a look at the conservation equations underneath. Applying the basic laws of flow physics, that is the conservation of mass, momentum and energy, to the viscous flow of ideal gas yields the Navier-Stokes equations. In integral tensor notations for solving steady-state problems they read as follows:

$$\frac{\partial}{\partial t} \int_{\Omega} \vec{U} \, d\Omega + \oint_{\partial\Omega} \vec{F}(\vec{U}) \cdot \vec{n} \, dS = \vec{Q}_{\Omega} \quad (1)$$

$\vec{U}$  contains the conservative variables of three-dimensional flow:

$$\vec{U} = \begin{pmatrix} \rho \\ \rho u \\ \rho v \\ \rho w \\ \rho E \end{pmatrix} \quad (2)$$

The flux density tensor  $\vec{F}$  is composed of the inviscid part  $\vec{F}^c$  (related to convection) and the viscous part  $\vec{F}^v$  (related to diffusion):

$$\vec{F} = \vec{F}^c - \vec{F}^v \quad (3)$$

Since both laminar and turbulent base numerics remain unaltered by the actuator disc implementation the flux density tensors don't need to be considered in more detail. However,  $\vec{Q}_{\Omega}$  on the right-hand side represents a vector of source terms. It is included in Equation (1) because the present actuator disc boundary condition implementation is based on a source term formulation.  $\vec{Q}_{\Omega}$  is equivalent to a formulation using a generic surface source tensor using the Gauss' divergence theorem as follows:

$$\vec{Q}_{\Omega} = \begin{pmatrix} \dot{m} \\ F_x \\ F_y \\ F_z \\ \dot{E} \end{pmatrix} = \oint_{\partial\Omega} \vec{Q}_S \cdot \vec{n} \, dS = \int_{\Omega} \text{div}(\vec{Q}_S) \, d\Omega \quad (4)$$

This equation is meant to show that there are different source term implementation possibilities. One may for instance want to use an existing helicopter grid. Then, one could prescribe the actuator disc geometry and determine all volume elements that are cut. In a second step appropriate volume source terms could be applied [6]. Although this approach would be independent of grid generator modifications it raises questions on an appropriate grid resolution in the disc vicinity. Thus, refining the rotor region would be necessary. The second approach utilizing surface source terms is based on a clearly defined actuator disc surface in the flow domain. Equation (4) shows that  $\vec{Q}_S$  in general may contain mass flow sources, force stresses and a power source term, where  $\vec{Q}_S$  may vary from control volume to control volume. The meaning of  $\vec{Q}_S$  is similar to the flux density tensor  $\vec{F}$ . In the case of an actuator disc that is supposed to model a rotor there will be shear stresses inducing swirl, normal pressure forces providing the rotor thrust and a power contribution. On mass conservation grounds the mass flow source term will be zero.

In the case of a finite volume scheme the discretization of the flow domain is performed by breaking it into small control volumes. Nodal flow variables represent the average over the control volume. Then, Equation (1) along with Equation (4) is cast into an expression in terms of the temporal change of the flow variables:

$$\frac{d}{dt} \bar{U} = - \frac{\int_{\partial\Omega} (\bar{F}(\bar{U}) - \bar{Q}_s) \cdot \bar{n} dS}{\int_{\Omega} d\Omega} \quad (5)$$

Later on and along with this equation it will be shown how source terms are applied. Although this work follows the source term approach it should be mentioned at this place that other attempts have been made. Instead of applying source terms as in Equation (5) the flow variables  $\bar{U}$  may directly be modified so as to impose the propulsion effect by prescribing a jump in pressure and tangential velocity. Le Chuiton [3] has tried several approaches and gives a comprehensive overview on different methods. However, he encountered stability problems for boundary conditions on variables and arrives at the source term approach. It is more robust because the force is directly fed into the flow field by means of source terms. This makes the arbitrariness of extrapolations that go along with boundary conditions on variables unnecessary, which is critical in regions of reversed flow on an actuator disc.

### **TAU Base Numerics**

The flow solver TAU utilizes a finite volume scheme to solve the Reynolds-Averaged Navier-Stokes equations (RANS) and offers turbulence modeling [7]. It incorporates both central and upwind schemes for the spatial discretization. Both steady and unsteady problems can be solved. Beneath the classical explicit Runge-Kutta relaxation scheme there exists a more modern quasi-implicit backward Euler method, LUSGS. Compared to the Runge-Kutta scheme it offers shorter computation times and better convergence. Convergence acceleration techniques such as multigrid, residual smoothing and low Mach number preconditioning are available. TAU is typically used in cell-vertex mode where the flow variables are stored at the primary grid vertices and fluxes are computed using the dual grid.

### **TAU Data Structure**

As having an unstructured scheme, TAU employs its own preprocessor for the transformation of the primary grid into the dual grid, which is used for computation [8].

Figure 1 is a simple 2D representation of the primary grid with a boundary dual control volume. The vertices of the primary grid coincide with the nodes of the dual grid, with the dual control volumes surrounding each node. The surface of a dual control volume is made up of individual faces, each of which belongs to one primary grid edge. Faces are characterized by their nor-

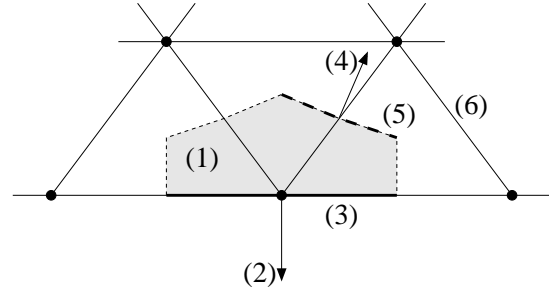


Figure 1: 2D representation of the boundary dual control volume (1) with the boundary face vector (2) and the boundary face (3), the example domain face vector (4) which belongs to the domain face (5) and a primary grid edge (6)

mal vector with its magnitude equaling the face area size. Figure 1 shows how primary grid edges and dual control volume faces are linked together.

Figure 1 is a simple 2D representation of the primary grid with a boundary dual control volume. It also shows how primary grid edges and domain faces are linked together.

Fluxes are computed face-wise by looping over all domain (primary grid) edges and residual contributions are added to their corresponding nodes. This ensures that all fluxes per dual control volume are taken into account making nodal residuals complete.

On the domain boundary, the dual control volumes are closed with respect to the boundary faces where the node is located directly on the boundary as can be seen in Figure 1.

This figure furthermore visualizes that a special treatment needs to be applied to boundary nodes. First of all, in terms of the data structure boundary faces are stored separately from the domain faces. Second, the domain flux scheme does not work on boundary faces. Boundary conditions therefore aim at providing either a special formulation of the boundary fluxes or a way of determining the flow variables themselves.

### **Concept: Zero Thickness Disc and Node Pairs**

The situation depicted in Figure 1 represents the way that boundary conditions need to be set up in TAU: the numerical flow domain is closed using boundary faces that carry no information about what is beyond. This makes it necessary to cover an actuator disc with boundary faces on top and bottom and close the disc watertight despite of its zero thickness.

In detail, such a disc is composed of border nodes, which belong to both the top and bottom surface, and two groups of nodes which make up these two boundary surfaces, as it is shown in Figure 2. These findings are based on thoughts and ideas of Axel Raichle at DLR.

The task now is to determine the exact boundary face

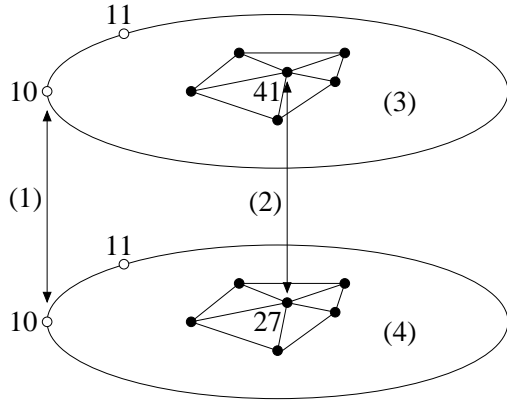


Figure 2: Numerical data structure representation of the actuator disc with example nodes IDs. Border nodes (1), node pairs (2) with different node IDs, the sides (3) and (4) with different boundary markers.

flux contribution to the residual of each actuator disc boundary node and to add source terms. Prior to adding the source terms a perfect through-flow condition must be provided. The idea is to exchange information of both actuator disc sides. This method, however, makes node pairs of top and bottom nodes at the same physical location mandatory. This also implies that corresponding boundary faces be identical except of their face vector orientation, which, of course, is opposite in sign.

Centaurusoft [9] implemented the zero thickness feature into their commercial grid generator according to the specifications by Axel Raichle. The two different actuator disc sides are stored separately with different boundary markers so that one can distinguish between nodes which belong to the top or bottom side.

To summarize, the data structure concept for an actuator disc in the unstructured TAU solver is as follows: there are two disc sides with different boundary markers which share the border nodes as can be seen in Figure 2. The pair nodes, however, exist on both sides at the same physical locations. Face vectors of all nodes belonging to one side have a counterpart on the other side with the same magnitude but opposite sign.

### Concept: Through-Flow Condition

The actuator disc approach does not take individual rotating blades with compressible flow phenomena into account. Regarding the Mach number regime therefore only the low subsonic regime where helicopters operate and the air can be assumed incompressible needs to be taken into account. Due to the essentially elliptic nature of this kind of flow the central Jameson scheme with classical dissipation is appropriate and has been chosen for this work.

A benefit of this scheme is that inviscid fluxes are calculated using only the two nodes that belong to a face.

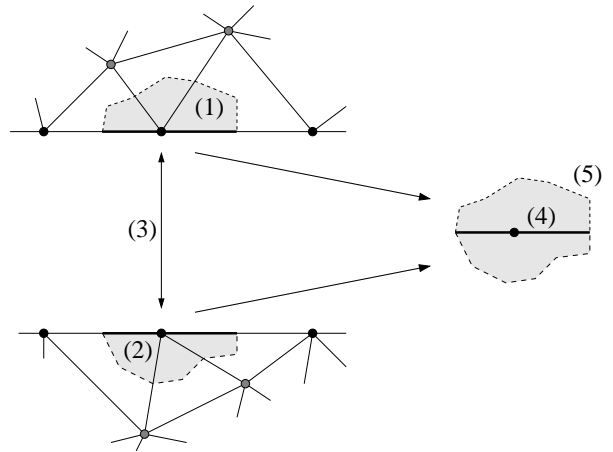


Figure 3: Treatment of separate dual boundary control volumes (1) and (2) as one complete dual control volume (4) via node pairs (3) with a closed outer surface (5)

That is, fluxes of the domain faces of an actuator disc are calculated correctly without any information of the other disc side.

Once the fluxes of all domain faces are computed and their contribution is added to the respective nodes a simple but exact through-flow condition is obtained as follows: since the dual control volumes of top and bottom pair nodes perfectly match together one only needs to add the two incomplete residuals together so as to obtain the exact through-flow residual. Figure 3 visualizes this concept.

This residual is then assigned to both nodes of the node pair. This procedure amounts to treating boundary nodes like domain nodes. Beneath simply adding residuals together, however, it has to be taken care of that node pairs are treated like one dual control volume throughout the whole solution process: both residuals, volumes and time steps need to be identical prior to relaxation. This is a way of ensuring that flow variables of node pairs remain identical.

This, for instance, made it necessary to adapt the smoothing algorithm for the Runge-Kutta relaxation. Low Mach number preconditioning and dissipation did not need to be changed.

### Concept: Actuator Disc Source Terms

Having tackled the through-flow condition the final step is adding source terms to the conservation equations. The discretized numerator of Equation (5) according to the Jameson scheme applied to TAU reads as follows:

$$\vec{R} = \left( \sum_{m=1}^{N_n} \vec{F}_m \cdot \vec{S}_m - \vec{D} \right) - \sum_{m=1}^{N_n} \vec{Q}_{S_m} \cdot \vec{S}_m \quad (6)$$

The big bracket on the right-hand side represents

fluxes computed by the central Jameson scheme with the dissipation vector to aid numerical stability. The summation over all source tensor contributions on the far right hand side reduces to a single expression since  $\bar{Q}_{S_m} \cdot \vec{S}_m$  is unequal zero only for one face per boundary control volume adjacent to the actuator disc surface:

$$-\bar{Q}_{S_{AD}} \cdot \vec{n}_{AD} S_{AD} = -S_{AD} \begin{pmatrix} 0 \\ f^x \\ f^y \\ f^z \\ \vec{f} \cdot \vec{V} \end{pmatrix} \quad (7)$$

As a first step the force vector  $\vec{f}$  for each actuator disc boundary node has been implemented as a pressure jump normal to the actuator disc as follows:  $\vec{f} = \Delta p \cdot \vec{n}$  so that the following relation is obtained:

$$-\bar{Q}_{S_{AD}} \cdot \vec{n}_{AD} S_{AD} = -S_{AD} \begin{pmatrix} 0 \\ n^x \Delta p \\ n^y \Delta p \\ n^z \Delta p \\ \Delta p \vec{V}_{AD} \cdot \vec{n}_{AD} \end{pmatrix} \quad (8)$$

This implementation served for debugging and verification purposes. Later on in this paper  $\vec{f}$  will be a real force distribution that needs to be provided by separate methods and is read from a file during the solver start.

## Verification

### Numerics Verification via Propeller Simulations

Prior to applying a pressure jump via source terms it has been checked that the through-flow condition works properly. With inactive source terms the L2 density residual is immediately at round-off error when computing free-stream flow through an actuator disc in an otherwise empty flow domain. That is, the actuator disc itself as a grid cut introduces no disturbance in the flow field.

For the verification of the source terms we shall consider test cases where the free-stream flow is perpendicular to the actuator disc. These cases are now referred to as propeller mode test cases. An actuator disc flow computation is initiated with free-stream flow and the source terms are active on the actuator disc. As the driving force they alter the pressure field and induce higher velocities at the actuator disc. Upon convergence, the flow field exhibits a propeller slip-stream with increased total pressure. Moreover, the pressure field around the actuator disc has adapted to the pressure jump across the actuator disc with lower pressure upstream and higher pressure downstream.

A simple 1D propeller theory for incompressible flow based on the momentum, Bernoulli and continuity equation that describes this kind of flow field exists

in the literature [10]. Applying Bernoulli's equation to the flow upstream and downstream of the disc and rearranging these relations gives an expression for the final stream velocity downstream of the actuator disc:

$$V_{\text{Stream}} = \sqrt{\frac{2\Delta p}{\rho} + V_{\infty}^2} \quad (9)$$

Applying the momentum equation gives a simple equation for the propeller thrust:

$$T = \dot{m} (V_{\text{Stream}} - V_{\infty}) = \Delta p \cdot A_{AD} \quad (10)$$

Along with the actuator disc mass flow  $\dot{m} = \rho \cdot A_{AD} \cdot V_{AD}$  the following expression for the actuator disc velocity is obtained:

$$V_{AD} = \frac{V_{\text{Stream}} + V_{\infty}}{2} \quad (11)$$

Finally, the continuity equation gives an expression for the stream contraction downstream of the disc:

$$\frac{d_{\text{Stream}}}{d_{AD}} = \sqrt{\frac{1 + \frac{V_{\text{Stream}}}{V_{\infty}}}{2}} \quad (12)$$

For the purpose of verifying that the actuator disc flow results comply with flow physics a comparison between 1D theory and actuator disc results has been drawn. Additionally, FLOWer results serve for comparison, too, since the same source term strategy is implemented there.

Several propeller mode test cases in Euler mode at different Mach numbers (from  $M = 0.2$  to  $M = 0.02$ ) and different thrust coefficients  $C_T$  have been computed and are reported in [11]. The thrust coefficient  $C_T$  is defined as follows:

$$C_T = \frac{T}{\rho_{\infty} (Rw)^2 A} = \frac{\Delta p A_{\text{eff}}}{\rho_{\infty} (c_{\infty} M_{\text{tip}})^2 A} \quad (13)$$

$A_{\text{eff}}$ , the area that the pressure jump is applied to, with  $A_{\text{eff}} = \pi (R^2 - R_i^2)$  is taken into account versus the reference area  $A$  with  $A = \pi R^2$ . This is because simulating real rotors is performed modeling the disc with a hole (of radius  $R_i$ ) at the center so that  $A$  and  $A_{\text{eff}}$  differ.

One example propeller mode test case, which is representative for the other cases, is shown here (with  $A = A_{\text{eff}}$ ). Flow solution data have been extracted along the axis of symmetry perpendicular to the actuator disc. This is most meaningful for a comparison to 1D theory.

Figure 4 shows both Mach number and pressure along the axis of symmetry of a flow case at  $M = 0.04$  and  $C_T = 0.006$  which translates into a pressure jump of 348.6 Pa for a free-stream pressure of 101,325 Pa.

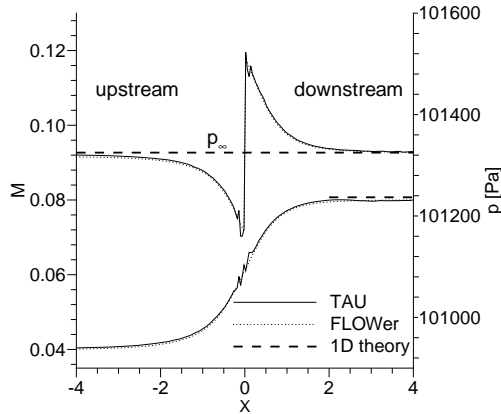


Figure 4: Comparison of pressure and Mach number curves at  $M = 0.04$ .

With low Mach number preconditioning turned on a high solution accuracy is obtained with the final slip-stream velocity close to 1D theory predictions. Moreover, the pressure jump across the disc is symmetric with respect to the free-stream pressure and exactly matches the input  $\Delta p$ . However, in contrast to FLOWer there are wiggles both in pressure and Mach number of the TAU solution. Since those wiggles remain bounded to the disc vicinity and do not change the characteristics of the curves they do not deteriorate the solution quality. One thing to note is that the TAU grid has been adapted once in the stream which increases the solution quality significantly. Comparing the TAU and FLOWer curves shows an excellent agreement and verifies the two source term implementation concepts, that differ in detail due to the difference between structured and unstructured flow solution strategies. Due to the low Mach number, convergence in TAU is limited to approximately five and a half orders of magnitude, which however is sufficient for an accurate representation of the pressure and velocity field.

Figure 5 shows a comparison of pressure fields and bounding streamlines for this case. Beneath the differences between a structured and an unstructured flow solution there is a good agreement between both pressure fields and bounding streamlines. This is also reflected by the stream contraction ratio which shows a relative error of approximately 2% compared to FLOWer and 1% compared to 1D theory:

	1D theory	TAU	FLOWer
$\frac{d_{Stream}}{d_{AD}} =$	0.865	0.873	0.856

### Rotor in Forward Flight

Now considering rotor in forward flight test cases

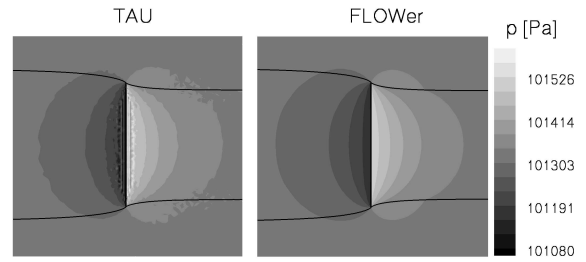


Figure 5: TAU and FLOWer pressure field and stream contraction at  $M = 0.04$ .

means essentially inclining the disc by only a few degrees up or down towards the on-flow. In this case, there exists no simple theory as for propeller mode cases. In contrast to the rather simple propeller flow rotor in forward flight cases are characterized by a rotor downwash as well as a strong vortex on each side of the disc. As well as in propeller mode, several test cases have been computed in Euler mode both in TAU and FLOWer and compared [11].

Figure 6, for instance, shows streamlines in a 2D plane perpendicular to the actuator disc at its downstream edge. The solutions have been obtained at  $M = 0.04$  and  $C_T = 0.006$  and the disc is rotated down by 7 degrees towards the on-flow. The TAU solution shows the disc left hand side while the corresponding FLOWer solution shows the right hand side. The streamlines in that 2D plane exhibit a very similar flow topology. In addition, the pressure in the vortex core drops to similar values. However, the vortex dissipates faster on the TAU grid since it has not been adapted in that case.

Figure 7 shows another test case at  $M = 0.1$  and  $C_T = 0.006$  at the same incidence as before. The pictures show both the Mach number and the total pressure gain fields with streamlines in a 2D plane parallel to the flow and perpendicular to the actuator disc. As before the flow fields resemble each other very well. Performing grid adaptation for the TAU actuator disc grid would further increase the solution quality.

Having computed both propeller mode and rotor in forward flight test cases has verified the numerical robustness and solution quality of both the TAU and FLOWer actuator disc implementation.

### Parallelisation

For the preparation of a primary grid for parallel flow computations the grid is partitioned into a user-defined number of domains. By default the geometric partitioner in TAU is used for that purpose which splits the grid applying geometric cuts. The resulting domains will typically form a regularly connected flow domain. Since the node pairs are the only additional data struc-

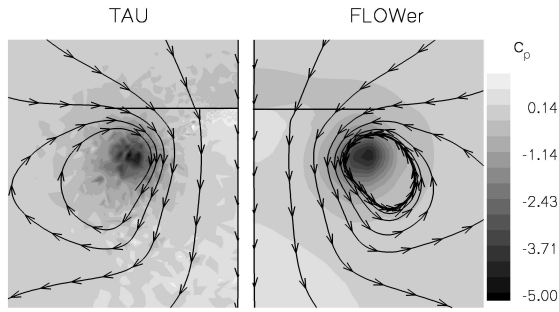


Figure 6: Vortex location visualized by  $c_p$  field and streamlines

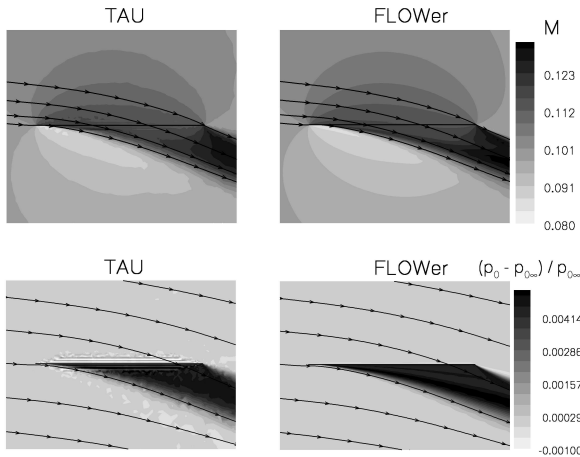


Figure 7: Downwash visualized by Mach number and relative total pressure gain fields

ture it must be ensured that the node pair connectivity is not destroyed due to partitioning. By definition, however, node pairs are at the exact same physical location. Using the geometric partitioner therefore nothing needs to be altered in the preprocessor since it is able to determine node pairs exactly in each domain. Moreover, it shows that due to the geometric partitioner all code parts that have been added to the solver also work in parallel automatically.

To confirm this a small isolated actuator disc flow case has been computed both in sequential as well as in parallel mode. It has been checked that partitioning splits the actuator disc into two parts in separate domains. Both physical flow results and convergence of the two cases match.

## Force distribution

The local on-flow conditions of rotor blades depend on a variety of parameters such that the resulting local force vector varies both with the radius and the rotation angle. Imposing a more realistic force distribution to the actuator disc shall therefore give more realism to the flow results.

Rotor codes, be they based on a solution of the Euler or Navier-Stokes equations or on simpler profile-database dependant methods, can be used to extract span-wise line loads as a function of the azimuth angle. Integration of that line load gives the overall rotor blade force at each azimuthal position  $F_{\text{blade}}(\psi)$ . Further integrating the rotor blade forces over an entire rotation and dividing by  $2\pi$  gives the average rotor blade force  $\bar{F}_{\text{blade}}$ :

$$\bar{F}_{\text{blade}} = \frac{1}{2\pi} \int_{\psi} F(\psi) d\psi = \frac{1}{T} \int_{t=0}^{t=T} F(t) dt \quad (14)$$

This relation, which is simply casting the integration over the angle by assuming a constant rotation frequency into an integration over time, shows that this kind of averaging gives the time-averaged rotor forces. It is the goal of an actuator disc force distribution to provide this time-averaged force.

Typically, rotor codes provide individual forces at varying radial positions for a certain amount of (equally spaced) azimuthal positions. Dividing the forces everywhere by the number of azimuthal stations therefore gives a time-averaged force distribution  $\bar{F}_{m,n}$ . The index  $n$  refers to azimuthal positions (ranging from 1 to  $N$ ) and the index  $m$  to radial positions (ranging from 1 to  $M$ ). The following equation is a discrete version of Equation (14):

$$\bar{F}_{\text{blade}} = \sum_{n=1}^{n=N} \left( \sum_{m=1}^{m=M} \bar{F}_{m,n} \right) \quad (15)$$

The interpolation from the structured grid given by the rotor code to the unstructured actuator disc grid in TAU must be performed utilizing force densities for the sake of staying conservative regarding the force  $\bar{F}_{\text{blade}}$ . That is, the structured grid is broken into non-overlapping surface fragments as can be seen in Figure 8 with an area discretized as  $A(m) = R(m) \cdot \Delta R(m) \cdot \Delta\psi$ . Bilinear interpolation of the force densities onto the actuator disc grid is followed by a transformation of the force density vectors from the rotor code coordinates to the TAU coordinate system [3].

A small interface program has been written that incorporates the three steps: time-averaging, interpolation and coordinate transformation. It is not included in the TAU source code since a clean interface to TAU is the surface grid file with the computation ready force distribution. This could make it easy to adapt the interface program to different rotor codes and empirically or experimentally provided force distributions. Thus, a wide range of applications ranging from propellers to rotors could be covered.

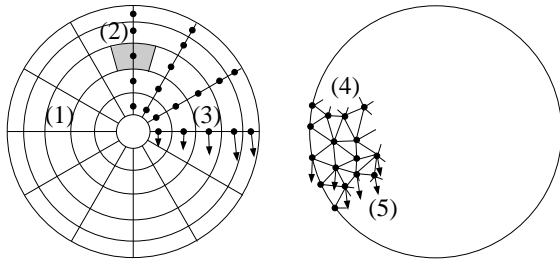


Figure 8: Forces are cast into force density vectors (3) on a structured grid (1) using the area (2). Interpolation and transformation yields force density vectors (5) on the unstructured actuator disc grid (4).

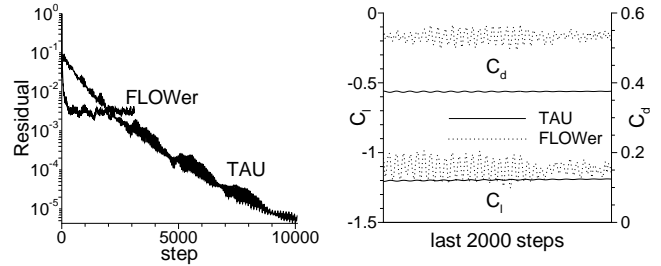


Figure 9: L2 density residual convergence of the EC145 case featuring a main rotor actuator disc force distribution with a comparison of  $C_l$  and  $C_d$  levels

## Interaction between main rotor and EC145 fuselage

A validation of the actuator disc boundary condition would be possible comparing numerical flow solutions to test flight data or wind tunnel measurements, in terms of PIV for example. However, since the experimental data of the EC145 helicopter are company property a comparison of numerical flow solutions obtained by TAU and FLOWer has been performed.

### Euler First Run

Prior to advancing to Navier-Stokes computations in TAU the flow around the EC145 helicopter has been computed in Euler mode first. Convergence of Navier-Stokes flow computations is typically limited due to viscous effects. Euler mode computations avoid these issues and enable to determine to what extent the interaction between main rotor and fuselage as well as main and tail rotor limit the convergence. Accordingly, a rather coarse Euler grid of the EC145 with approximately half a million grid nodes featuring a main and tail rotor actuator disc was generated using the commercial Centaur grid generator. The flow test conditions were as follows:

$M_\infty$	$\alpha_{\text{Fuselage}}$	$\alpha_{\text{AD main}}$	$C_{T \text{ main}}$	$C_{T \text{ tail}}$
0.2081	$0^\circ$	$-5^\circ$	0.007673	0.008927

Since the multigrid agglomeration algorithm in the TAU preprocessor had not yet been adapted to the needs of the actuator disc implementation, this flow case was computed in single grid mode. Nevertheless, the flow solution converged to machine zero despite of the small gap between main and tail rotor. This indicates that the actuator disc source term implementation can handle disturbed on-flow conditions.

### Navier-Stokes Run

With the experience of which flow features are to be

expected the final Navier-Stokes grid was generated featuring a total number of 4.06 million nodes, 108286 surface points and 20263 main rotor actuator disc nodes. Volume grid sources are placed in the grid to ease later vortex capturing as well as the flow between fuselage and empennage. The boundary layer grid is made up of 30 prism layers with an initial spacing of 0.01 millimeters in average. However, prism layer chopping as well as layer contraction was unavoidable with the Centaur grid generator due to CAD issues in some corners which definitely reduces the boundary layer resolution. Nevertheless, the non-dimensional wall-distance  $y^+$  is around one on the whole fuselage surface considering the flow solutions presented later on. The structured FLOWer grid [5] in contrast is made up of 8.28 million nodes, 80664 surface points and 8192 main rotor actuator disc nodes. Especially the resolution normal to the actuator disc is better with a much lower initial spacing.

Using the Runge-Kutta relaxation technique in single grid mode has shown to cause severe convergence problem. Instead, LUSGS has been tried as relaxation solver with the residual dropping to a significantly lower level on the present TAU grid.

Figure 9 shows the convergence of the L2 density residual as well as the integral coefficients  $C_l$  and  $C_d$  (with a reference area of  $1m^2$  both for FLOWer and TAU). The corresponding computations were performed at the same conditions as above with a Reynolds number of  $Re = 4.33$  millions, a main rotor actuator disc force distribution and a constant pressure jump on the tail rotor actuator disc. The turbulence models used were the Spalart-Almaras one-equation model in TAU and the LEA- $k\omega$  two-equation model in FLOWer. Similar solver settings with the central Jameson scheme as well as the identical force distribution have been applied.

Figure 10 shows the TAU force distribution in terms of force density vectors (aerodynamic forces acting on the actuator disc) that have been generated according to the method described previously. Force vectors are pointing down where the retreating blade faces re-

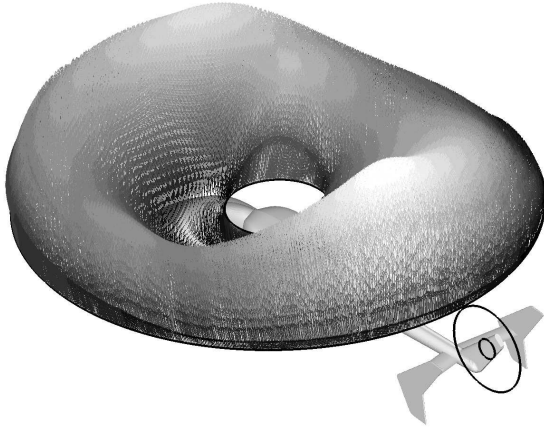


Figure 10: TAU force density vector distribution on the main rotor actuator disc

versed flow and thus produces negative lift. For comparison purposes these computations were rerun at the same flow conditions on each code with the actuator discs turned off.

Figure 11 shows corresponding pressure iso-surfaces on top of the EC145 fuselage. Globally, both flow results resemble each other quite well while there are noticeable differences on the tail horizontal stabilizer. Vortices emanating from the fuselage are more pronounced in the FLOWer case such that they leave a trace on both sides of the horizontal stabilizer. A more detailed view on different flow phenomena becomes evident in Figure 12.  $c_p$ -curves of the top surface center line are plotted along with the fuselage shape as a reference for the observed peaks in pressure. Both TAU solutions exhibit wiggles which are due to an insufficient surface grid resolution. Indeed, those wiggles also appear in the surface shape while zooming in closely. Nevertheless, corresponding TAU / FLOWer  $c_p$  curves match quite well in regions of attached flow. That is, from the nose to the engine inlet and on the tail vertical fin. A clear difference in  $c_p$  is noticeable for computations with versus without actuator disc.

However, the flow is largely dominated by vortices between the engine inlet and the tail vertical fin with a strong impact on the  $c_p$  curves. This also explains the differences in  $C_d$  as can be seen in Figure 9. Locally, this effect is especially pronounced behind the cabin on the tail boom where differences due to the turbulence models as well as the grid density largely influence the trace of the flow separation. Figure 13 reveals vortex traces on top of the tail boom in the FLOWer case which do not appear in the TAU case.

Differences in vortex positions caused by the actuator disc therefore have a stronger impact on the  $c_p$  curves shown in Figure 12 as the pressure difference caused

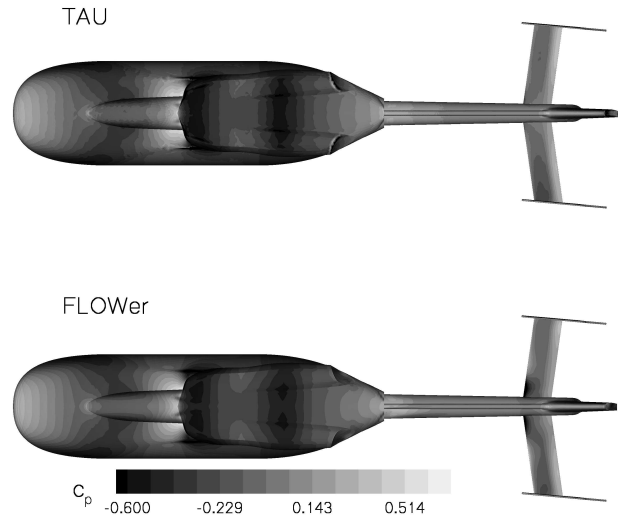


Figure 11: Comparison of  $c_p$  iso-surfaces on the EC145 fuselage top surface

by the actuator disc alone.

To complete the findings on the helicopter fuselage Figure 14 shows a comparison of the difference in  $c_p$  due to the actuator discs between FLOWer and TAU. It shows that the effect of the actuator disc on the surface pressure in attached flow regions is a little bit stronger in TAU than in FLOWer. Figure 14 furthermore shows that it is utmost important to be able to predict the effects of flow separation accurately since those are dominant on the tail boom. A more detailed CFD investigation of the EC145 fuselage with special emphasis on the interaction between vortices and the empennage by applying different solvers and turbulence models is reported in [12].

Last, but not least, the flow field in terms of vorticity and relative total pressure loss on a cut plane at  $x = 8$  m shall be discussed. Figure 15 and 16 show that despite global similarity flow features are captured sharper in FLOWer and appear to be more diffused in TAU. The tip vortices in Figure 15, for instance, are more compact in the FLOWer solution and there are several vortex sheet layers. In addition, the vorticity pattern around the tail boom exhibits noticeable differences compared to the TAU solution. It is assumed that these differences are due to both the turbulence model used and the much higher grid density in the FLOWer case. Performing several grid adaptation steps in TAU would be necessary to capture those details better. Adaptation has not been performed since the present TAU version is a development version where some solver features such as multigrid and adaptation have not yet been adapted to the needs of the actuator disc implementation.

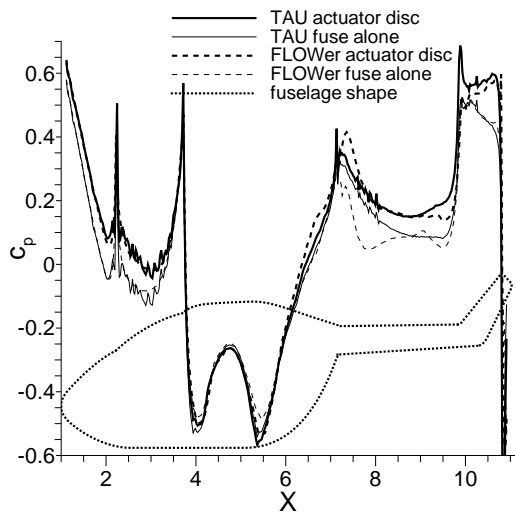


Figure 12: Comparison of the EC145 fuselage top surface centerline  $c_p$  curves

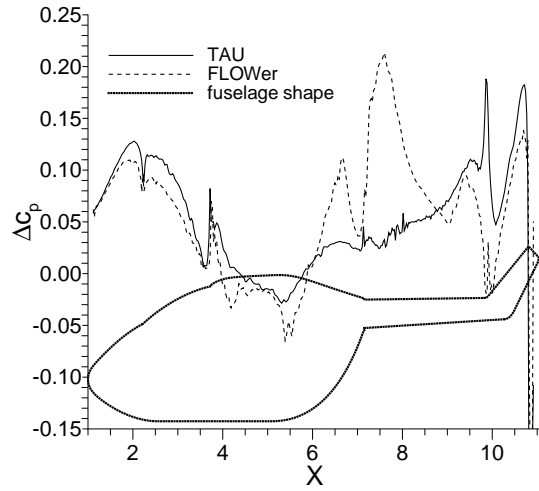


Figure 14: Comparison of curves of  $c_p$  difference between the fuselage alone and actuator disc case on the top EC145 fuselage top surface centerline

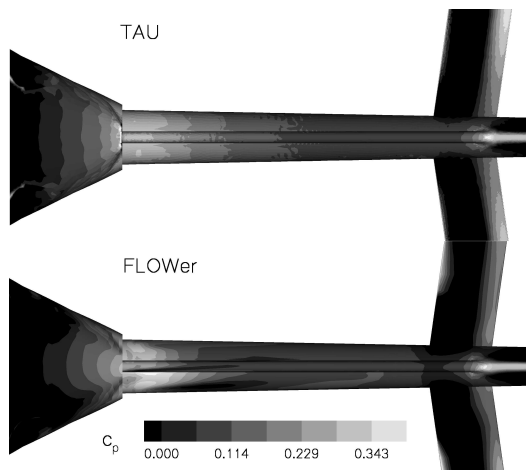


Figure 13: Comparison of  $c_p$  iso-surfaces on the EC145 top tail boom surface

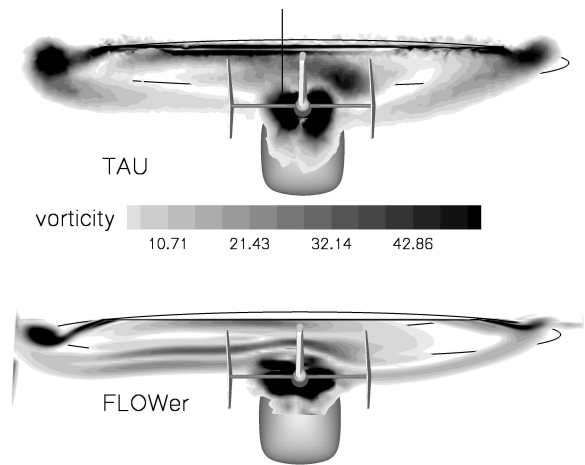


Figure 15: Comparison of relative total pressure loss iso-surfaces on a cut plane at  $x=8m$

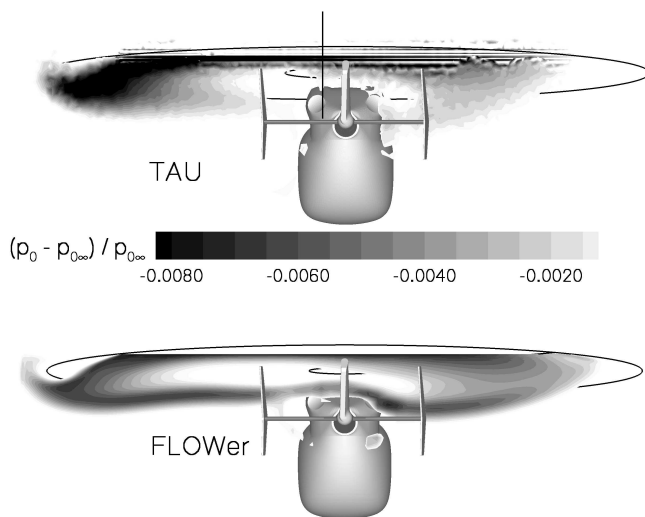


Figure 16: Comparison of vorticity iso-surfaces on a cut plane at  $x=8m$

## Conclusion

An actuator disc boundary condition suited for the time-averaged flow simulation of helicopter rotors in forward flight has been developed and implemented into the unstructured DLR flow solver TAU. The approach previously implemented into the structured DLR flow solver FLOWer was transferred to the unstructured framework. It is based upon a disc of zero thickness composed of two disc sides where the information exchange from one disc side to the other is performed using pairs of nodes at the same physical location. This enables the formulation of an exact through-flow condition augmented by energy and momentum source terms which impose the time-averaged effect of the rotor. Comparing pressure and Mach number field as well as the stream contraction ratio to FLOWer and 1D theory verified propeller flow simulations. Moreover, rotor in forward flight cases prove the robustness of the implementation and resemble FLOWer results. An interface has been written that casts line loads of isolated rotor blade simulations into a force distribution for the whole actuator disc. The force distribution in terms of force density vectors is directly used as input for the source terms in TAU. The viscous flow field of the EC145 helicopter has been computed in parallel with a force distribution of this kind and a comparison to FLOWer has been drawn. It shows that there is good agreement between the two codes in predicting the effect of the actuator disc on the fuselage pressure distribution. However, a big portion of the flow is dominated by vortices emanating from the fuselage and the position of those vortices is altered by the rotor downwash. This makes a

high grid resolution and high-quality turbulence models for a more realistic flow field computation mandatory. Future work will address the integration of the actuator disc implementation into the central TAU version and could involve the implementation of a trim procedure by considering flight mechanics and coupling the main rotor force distribution to a rotor code.

- [1] Pahlke, K. "Berechnung von Strömungsfeldern um Hubschrauberrotoren im Vorwärtsflug durch die Lösung der Euler-Gleichungen", DLR-Forschungsbericht 1999-22, ISSN 1434-8454, 1999.
- [2] Stangl, R. "Ein Euler-Verfahren zur Berechnung der Strömung um einen Hubschrauber im Vorwärtsflug", Herbert Utz Verlag Wissenschaft, ISBN 3-89675-141-7, München, 1996.
- [3] Le Chuiton, F., "Actuator Disc Modelling for Helicopter Rotors", Aerospace Science and Technology, Vol. 8, No. 4, June 2004.
- [4] Bettshart, N., "Rotor Fuselage Interaction: Euler and Navier-Stokes Computations with an Actuator Disk", AHS 55th Annual Forum, Montreal, Canada, May 1999.
- [5] D'Alascio, A., Pahlke, K. and Le Chuiton, F., "Application of a Structured and an Unstructured CFD-Method to the Fuselage Aerodynamics of the EC145 Helicopter. Prediction of the Time Averaged Influence of the Main Rotor", ECCOMAS, Jyväskylä, Finland, July 2004.
- [6] Rajagopalan, R.G., Mathur, S.R., "Three Dimensional Analysis of a Rotor in Forward Flight", Journal of the American Helicopter Society, pp. 14-25, July 1993.
- [7] Kroll, N., Rossow, C.C., Becker, K. and Thiele, F. "MEGAFLOW - A Numerical Flow Simulation System", 21st ICAS Congress, Melbourne, paper 98-2-7.3, 1998.
- [8] "Technical Documentation of the DLR TAU-Code", DLR, Institute of Aerodynamics and Flow Technology, Braunschweig, June 2004.
- [9] [www.centaurosoft.com](http://www.centaurosoft.com)
- [10] Schröder, W. "Fluidmechanik", Aachener Beiträge zur Strömungsmechanik, Band 3, 2. Auflage, Wissenschaftsverlag Mainz in Aachen, Aachen, 2000.
- [11] Schweikhard, R. "Implementation and Validation of an Actuator Disc Boundary Condition for Helicopter Rotors into the Hybrid DLR RANS

Solver TAU”, DLR IB 124-2004/27, ISSN 1614-7790, 2004.

- [12] D’Alascio, A., Castellin, C., Schöning, B. “Investigation of the Effect of Advanced Turbulence Models on Blunt Helicopter Fuselages”, 31st European Rotorcraft Forum, Florence, Italy, 2005.